

Jun Porcelain-Like Birefringent Supramolecular Film for Multiple Logic Data Storage

Tongyue Wu, Peilong Liao, Jinwan Qi, Shuitao Gao, Ting Gu, Jianbin Huang, and Yun Yan*

Information security is of predominant significance, while multiple logic information encryption techniques remain challenging. Here it is reported that upon coupling the unduplicable Jun Porcelain-like birefringence and it enables polarized fluorescence with solid phase molecular self-assembly (SPMSA), multiple logic information encryption can be achieved upon correctly applying UV light and polarizing angles. Since each birefringence is unique and can be transformed into a corresponding digital bar code, the multiple logic can be further encrypted with the assistance of a digital bar code bank, thus yielding the ultimate information security.

1. Introduction

Information security is of significant importance for the safety of the economy, military, and politics.^[1] Over the past centuries, a wide variety of anti-counterfeiting technologies have been developed,^[2] such as watermarks,^[3,4] intaglio printing,^[5] luminescent ink,^[6,7] and anti-counterfeiting paper.^[8,9] However, anti-counterfeiting marks based on these techniques can be forged vividly.^[10,11] Because the patterns are the same for products of the same batch, it is difficult to tell an authentic copy from the vividly-faked one. For this reason, it has been an eternal campaign to fight against counterfeiting.

Compared with those designs that can be duplicated easily, the pattern of the Chinese Jun Porcelain, which is prospered in the Song Dynasty, is very unique, and no two Jun Porcelain potteries have the same patterns. This is because the pattern is naturally occurred as the minerals are heated in a kiln, where the mineral dyes in the outer-layer fill in the irregular burning cracks

generated in the underlayer. This inspires that if the anti-counterfeiting patterns are made as unique as Jun Porcelain, duplication would become very difficult. However, this seems illusive due to the difficulties in creating such unique patterns.

Birefringence is a phenomenon in which incident light in an anisotropic material splits into two refractions.^[12–15] Recently, some anisotropic birefringent materials have been reported,^[16] such as cellulose nanocrystal (CNC)-containing film^[17–19] and clay orientated hydrogel.^[20] Owing to the large size and well-defined geometry of

these static nanoparticles, the birefringence yielded in these films is very limited, and the pattern and color of the film can be well-controlled through orientation and thickness manipulation.^[18,20–24] However, if the birefringence comes from dynamic molecular assemblies, the birefringence would become more complicated, since it is hard to generate exactly the same orientation, size, and geometry of self-assembled domains.^[25–28] This inspires that such birefringence is in high analogy to the pattern of Jun Porcelain, which is probably possible to be employed to create unduplicable anticounterfeiting techniques.

Herein we report that unduplicable Jun Porcelain-like birefringence may indeed come true through solid-phase molecular self-assembly (SPMSA). In SPMSA, a supramolecular plastic film is created by mechanically pressing the precipitates formed with a pair of oppositely charged surfactants and polyelectrolyte.^[29–34] Owing to the presence of hydrophobic surfactant domains with arbitrary thickness and orientations, the resultant supramolecular films are anisotropic. Upon stretching, alignment and rearrangement of these hydrophobic bilayers may occur, but the status of these changes is case and site-dependent owing to the difficulties of molecular arrangement in solid phases. Furthermore, the alignment of the bilayers also yields polarization of lights, so that fluorescent dyes in the birefringent film display angle dependent fluorescence. By integrating bilayers with different birefringent properties and doped fluorescent dyes, authentic information can be revealed only by correctly coupling UV, visible light, and polarizing angles. Plus the fact that each birefringence pattern can be assigned a unique digital code, we are able to create a Jun Porcelain-like multiple logic information encryption technique which is very promising in the broad field of economy, politics and military.

T. Wu, P. Liao, J. Qi, S. Gao, T. Gu, J. Huang, Y. Yan
Beijing National Laboratory for Molecular Sciences (BNLMS)
College of Chemistry and Molecular Engineering
Peking University
Beijing 100871, P. R. China
E-mail: yunyan@pku.edu.cn

Y. Yan
Ningxia Key Laboratory of Green Catalytic Materials and Technology
College of Chemistry and Chemical Engineering
Ningxia Normal University
Guyuan 756000, P. R. China

 The ORCID identification number(s) for the author(s) of this article can be found under <https://doi.org/10.1002/adom.202403382>

DOI: 10.1002/adom.202403382

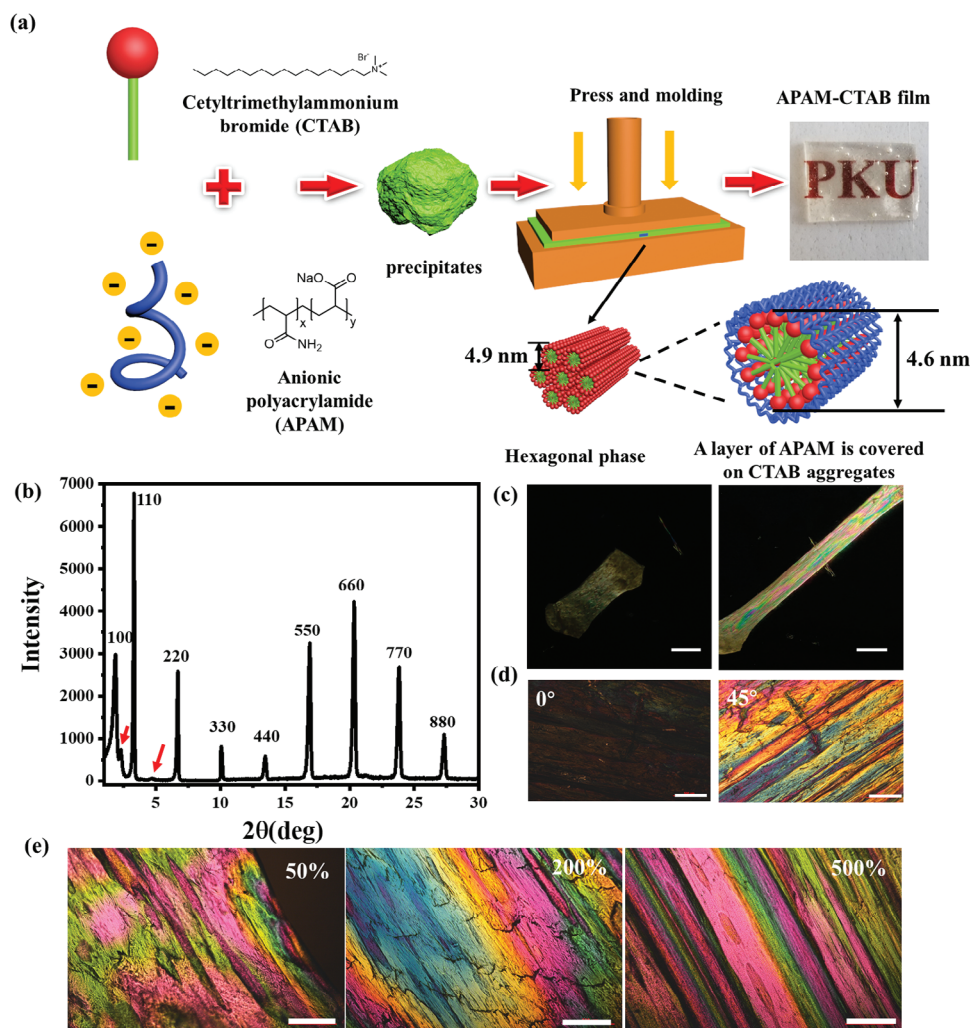


Figure 1. Characterization of basic structure and properties of APAM-CTAB film. a) Systematically illustration of the preparation method of APAM-CTAB film. b) XRD results of APAM-CTAB film, lamellar phase, hexagonal phase, and CTAB crystal coexist in the film. c) The birefringence of the pristine (left) and stretched (right) films between two orthogonally placed polarizers (Scale bar: 2.5 cm). d) The birefringence of the films was observed by a polarizing microscope (POM) under 400% tensile strength (Scale bar: 500 μm). e) The birefringence of the films was observed under a polarizing microscope (POM) under different tensile strengths of 50, 200, and 500% (Scale bar: 500 μm).

2. Results and Discussion

2.1. Preparation and Characterization of APAM-CTAB

The Jun Porcelain-like birefringence was generated from the supramolecular film of APAM-CTAB, where APAM and CTAB are the anionic polymer [anionic polyacrylamide] and cationic surfactant [cetyltrimethylammonium bromide], respectively. **Figure 1a** illustrates the solid phase molecular self-assembly (SPMSA) procedure of the APAM-CTAB film, which is an effective method for building supramolecular films proposed by us.^[30,33,34,32] First, the aqueous solutions of APAM and CTAB were made. Upon mixing the two at the charge concentration of $[+]:[-] = 1:1$, precipitates were generated immediately. Under the mild pressure of 5Mpa and preserving at the relative humidity (RH) of 100% for 8 h, a transparent film with stretchability over 600% (Figure S1, Supporting Information) was obtained.

XRD measurements in the low angle region of $1\text{--}5^\circ$ (Figure 1b) display two strong diffractions with a spacing ratio of $1:\sqrt{3}$, corresponding to the (100) and (110) Miller Indices of a 2D hexagonal mesostructure.^[35–37] The distance obtained from the 100 diffraction is 4.9 nm, which is slightly larger than the two times the extending length of CTAB (4.6 nm). This means that the APAM chains have electrostatically bonded to the head group of CTAB, resulting in a longer hydrophilic section. These APAM covered CTAB molecules then form worm-like micelles (Figure 1a). There is also a group of weaker diffractions with a spacing ratio of 1:2 (red arrows in Figures 1b and S2 (Supporting Information), separated XRD in small angle region and enlarged (002) diffractions), corresponding to the (001) and (002) Miller Indices of a 2D lamellar phases of CTAB with the thickness of 3.8 nm.^[35–37] It is noticed that the peaks in the high angle region are all the multi order diffractions of the (110) face of the hexagonal phases, indicating the CTAB molecules

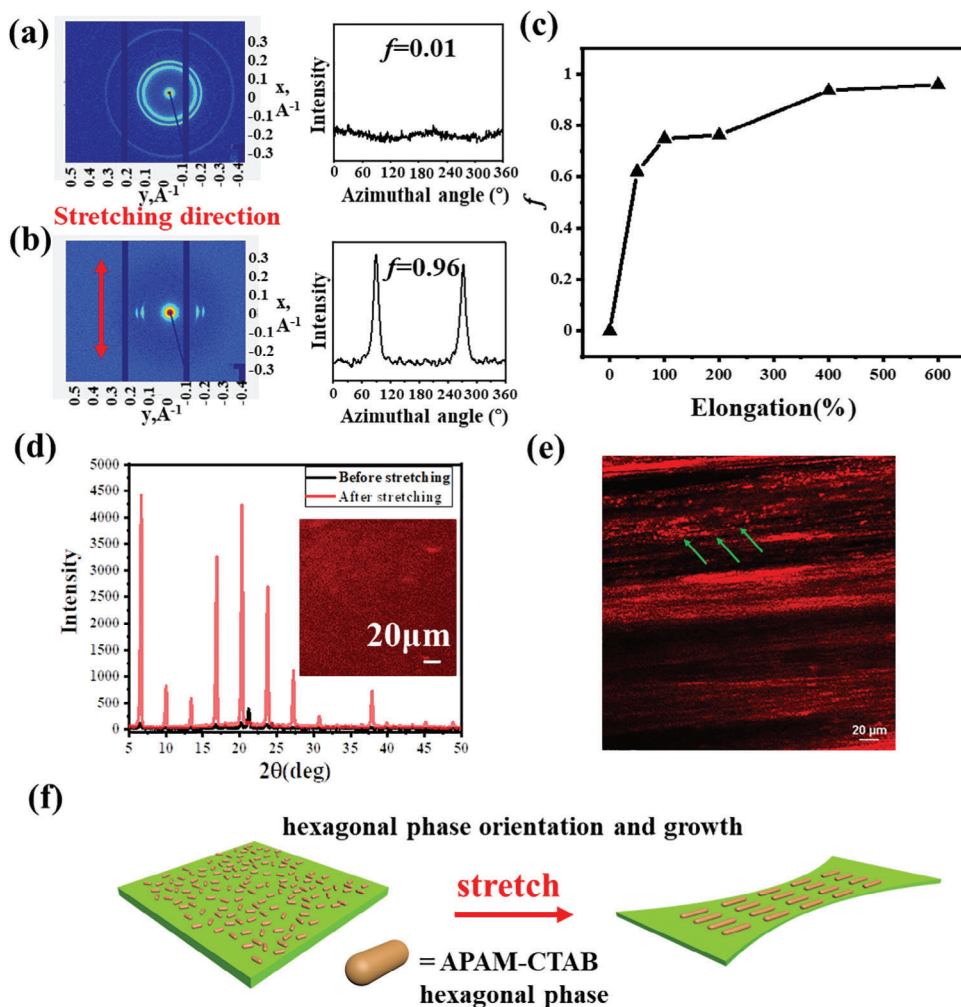


Figure 2. a) Medium Angle X-ray Scattering (MAXS) analysis of the original film and b) 600% stretched film with calculated orientation order parameter (f). c) Plot of orientation order parameter (f) relative to elongation ratio. d) 1D-XRD of APAM-CTAB film before and after stretching. Inset is the CLSM image of the unstretched film. e) CLSM result of Nile red stained APAM-CTAB hexagonal phase after stretching. (Arrows: APAM-CTAB hexagonal phase) f) Schematic diagram of APAM-CTAB hexagonal phase orientation and alignment upon stretching.

interacting with APAM have predominantly arranged into worm-like micelles which further packed hexagonally in the film (Figure 1a), and only a small fraction of CTAB molecules arrange into lamellar phases (Figure S2, Supporting Information).

Both the sizes of the hexagonal phases and the lamellar phases in the original film are not comparable to the wavelength of the visible light, since the film has very weak birefringence (Figure 1c, left). However, as the film is stretched uniaxially, the birefringence becomes very significant (Figure 1c, right). The intensity of the birefringence is the strongest at the aligning angle of 45° and 135° , but is the weakest at the angle of 0° and 90° (Figures 1d and S3, Supporting Information, the complete POM figure), which features the birefringent behavior of a polarizer with one uniform axis. Remarkably, the birefringent color and patterns vary significantly as the film stretched to different extents (Figures 1e and S4, Supporting Information, POM for other stretching extent), indicating the continuous alignment of the mesophases with stretching.^[38] This birefringence phenomenon has good humidity and storage stability. Figure S5 (Supporting

Information) shows the POM observation results of the same film under different humidity and long-term placement with no significant changes observed. It is noticeable that the birefringence is not from APAM. According to Figure S6 (Supporting Information), both the APAM solution and film show no birefringence. In addition, similar birefringence results of APAM-DTAB (C12) film and APAM-STAB (C18) film are shown in Figure S7 (Supporting Information), indicating a universal birefringence phenomenon in APAM-surfactant films.

2.2. Stretching Induced Orientation of the Mesophases in the Film

The above results strongly manifest that the CTAB mesophases have oriented upon stretching, and the extent of orientation keeps increasing upon stretching, which can be clearly reflected in the changes in the 2D XRD pattern. Figure 2a shows that concentric circles were observed for the pristine unstretched

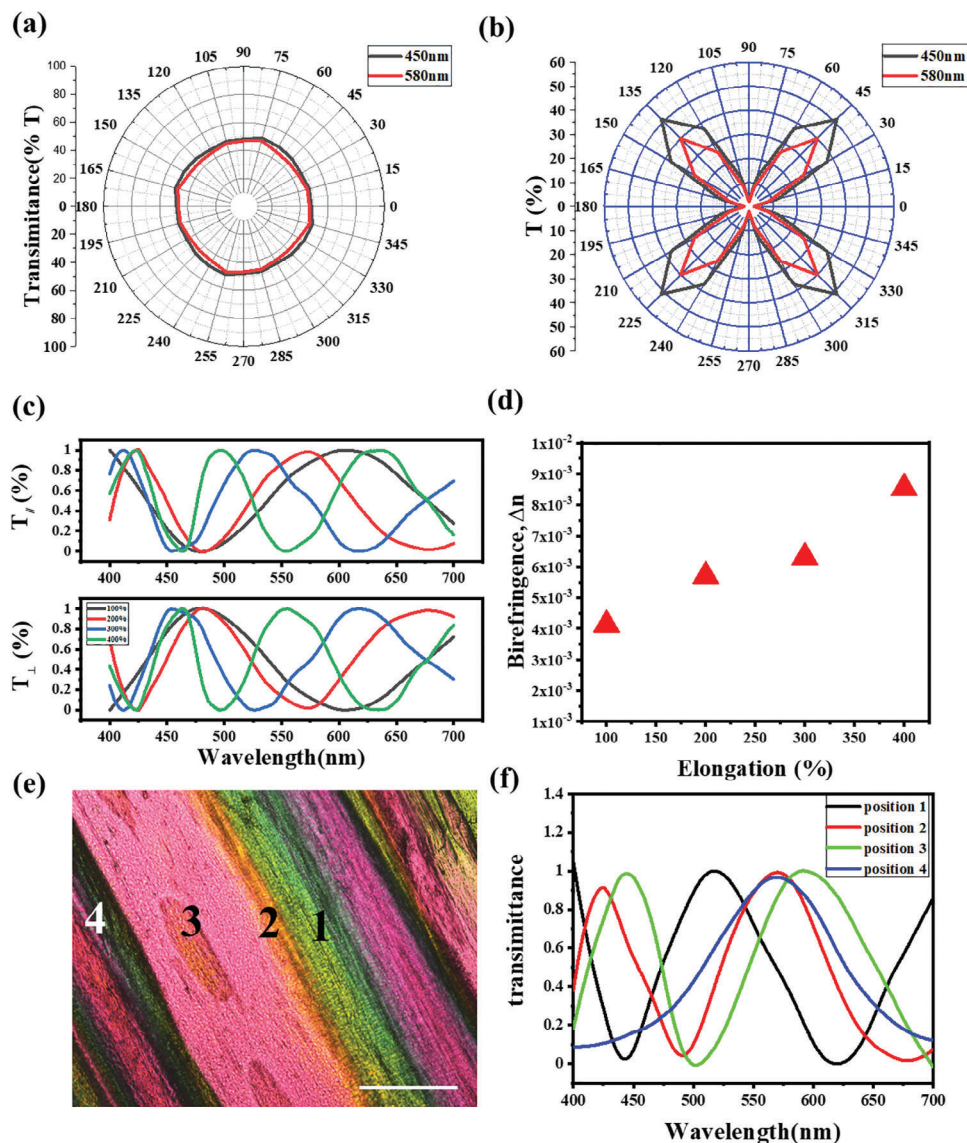


Figure 3. Polarized ultraviolet-visible (UV-vis) spectroscopy of APAM-CTAB film. a,b) Transmittance of the film before (a) and after (b) stretching. c) Polarized UV-vis spectra of APAM-CTAB film with different stretching degrees. d) Birefringence increases as the sample is stretched. e) Labeling four different birefringence colors in a stretched film. f) UV-vis spectra for the four positions in (e) with polarizer and analyzer in cross direction. (The stretching direction of samples is oriented 45° relative to the polarizer unless otherwise noted.) (Scale bar: $500 \mu\text{m}$).

APAM-CTAB film, whereas the ring was replaced by short arcs after stretching (Figure 2b), unambiguously verified the alignment of the oriented CTAB hexagonal phases.^[20] To quantify the extent of CTAB alignment, we calculated the orientation order parameter (f) ($0 \leq f \leq 1$, introduced by Equations (1)–(3)) based on the diffraction intensities at $2\theta = 1.88^\circ$ ($q = 0.143 \text{ \AA}^{-1}$).^[39]

$$I = I_0 + A \exp[\omega \cos^2(\varphi - \varphi_0)] \quad (1)$$

$$f = \frac{\int_{-1}^1 P_2(\cos \varphi) \exp(\omega \cos^2 \varphi) d(\cos \varphi)}{\int_{-1}^1 \exp(\omega \cos^2 \varphi) d(\cos \varphi)} \quad (2)$$

$$P_2(\cos \varphi) = \frac{1}{2} (3 \cos^2 \varphi - 1) \quad (3)$$

where I_0 denotes the free baseline intensity, φ_0 is the azimuth at the position of the maximal intensity, φ is the azimuth and ω is the parameter that determines the width of the distribution. After the curve fitting of this function to the azimuthal angle plot, parameters I_0 , A , and ω were obtained. The orientation order parameter f was determined using Equation (3).

We determined $f = 0.01$ for the pristine APAM-CTAB film, indicating a negligible anisotropy in the film. In contrast, the orientation order parameter (f) increased as APAM-CTAB film was stretched, and up to the largest value of $f = 0.96$ at 600% elongation (Figure 2b,c). Since the maximum f value is 1, this large f indicates that the internal hexagonal structures of the film are almost completely aligned. It is noticed that the

diffraction peaks in the 1D XRD spectra are significantly intensified and sharpened (Figure 2d), indicating the increased extent of periodicity of ordered structures, which may be the result of an increase in crystal size^[40] and crystal orientation.^[41] Herein, the 1D XRD pattern in Figure 2d is in perfect agreement with the $\approx 100\%$ alignment of the hexagonal phases observed in the 2D XRD, which can be clearly observed under CLSM (Figure 2e). In contrast, no discernable alignment can be observed for the unstretched pristine film (Inset in Figure 2d). The orientational alignment of the CTAB hexagonal phases triggered by the stretching of the film is schematically illustrated in Figure 2f.

2.3. Polarized Optical Properties of the Stretched APAM-CTAB Film

The APAM-CTAB with highly oriented hexagonal phases displays polarized optical properties, which can be clearly evidenced by the polarized ultraviolet-visible (UV-vis) spectroscopy measurements. The angle between the polarizer and analyzer was fixed at 90° , and the film placed between them was stretched along the direction of 45° ($\theta = 45^\circ$) under a spot of 0.3 cm. (Figure S8, Supporting Information, set-up illustration of the measurement). The original unstretched APAM-CTAB film transmitted light without angular dependence in the range of 400–700 nm (Figures 3a and S9, Supporting Information), but anisotropy emerged gradually as the sample was stretched (Figures 3b and S10, Supporting Information). Moreover, the spectra were inverted as the polarizer and analyzer were placed parallel to each other (Figure S11, Supporting Information), resulting in the complementary color. This unambiguously confirms that the anisotropy of the birefringence is caused by the stretching.

According to the definition of birefringence, in a typical birefringent material that has one optical axis, the transmitting polarized light intensities measured between crossed and parallel polarizers can be described by Equations (4) – (5) that depend on the orientation of the optical axis (i.e., the stretching direction of APAM-CTAB film in this study), where d is the sample thickness, λ is the wavelength and Δn is the birefringence.^[42]

$$I_{\perp} = \sin 2\theta \sin^2 \frac{\pi d \Delta n}{\lambda} \quad (4)$$

$$I_{\parallel} = \sin 2\theta \cos^2 \frac{\pi d \Delta n}{\lambda} \quad (5)$$

Figure 3c shows that the period of the transmittance keeps decreasing while the average birefringence (Δn) keep increasing (Figure 3d) as the film is stretched. However, the birefringence (Δn) is site specific in the film. As 4 sites within the 0.3 cm optical spot were selected (Figure 3e), both the measured Δn (Table 1) and transmittance (Figure 3f) are drastically different from each other. This result unambiguously disclosed that the 3D size of the hexagonal APAM-CTAB mesophases is not uniform upon stretching. We consider this is because the size of the pristine CTAB mesophases is rather heterogeneous due to the fast electrostatic interactions between CTAB and APAM, and this inhomogeneity would directly yield molecularly heterogeneous thickness of the stretched APAM-CTAB film due to the slow molecu-

Table 1. Birefringence at different positions.

Position	Birefringence (Δn)
1	0.0056
2	0.0057
3	0.0061
4	0.0038

lar diffusion in a solid phase. Since the extending chain length of CTAB is ≈ 2.3 nm, it has a drastic impact on the refringence behavior of the film and yields different birefringence patterns. Even if the stretching speed and rate are carefully controlled, it is almost impossible to obtain CTAB mesophases of exactly the same thickness in the entire film. As a result, the birefringence would be site specific, and it is unduplicable (Figure S12, Supporting Information).

2.4. Multi-Mode Anti-Counterfeiting Application

The unduplicable site-specific birefringence is exactly like the unique patterns that happened to Jun Porcelain. The information included in the birefringence pattern can be divided into two parts: color and strip width with corresponding assigned numbers (Figure 4a). Thus, each birefringent pattern has a unique encoding sequence number (Figure 4b), similar to barcodes used in daily life. Upon being uploaded into a data pool, each of the numbered patterns can be digitally interpreted for authentic checks.

Moreover, the birefringence can be made even more complicated by overlaying two stretched APAM-CTAB films at different angles. It is noticed when the two films are stacked at an angle other than 90° , the birefringence color will change continuously with different aligning angles, as demonstrated in Figure 5a, and no darkening can be observed no matter how the film is aligned and how the two polarizers are arranged (Figure S13, Supporting Information).

With this design in mind, we choose one of the overlaid stretched films to create unduplicable birefringent security labels. Figure 5b shows an array composed of both the overlaid stretching and original APAM-CTAB films. Under ambient light, all the small squares show exactly the same characteristics, which cannot be distinguished from each other. However, under polarized light, a “C” birefringence anti-counterfeiting pattern can be obtained. Furthermore, the birefringent anticounterfeiting pattern can be upgraded by incorporating polarized fluorescence. Because of the birefringent feature of the overlaid film, the doped fluorescent dye would only give strong fluorescence at specific angles where the transmittance is the largest, which corresponds to the weakest birefringence. Figure 5c shows that the film gives normal fluorescence as the dye CBS (2,2'-([1,1'-Biphenyl]-4,4'-diylidene-2,1-ethenediyl)bis-benzenesulfonic acid disodium salt was doped into the film. However, the fluorescence becomes the strongest at the angle of $0^\circ, 90^\circ, 180^\circ$, and 270° and the weakest at the angles of $45^\circ, 135^\circ, 225^\circ$, and 315° (Figure 5d; Figure S14, Supporting Information). Other dyes such as Rhodamine B (RB) and Nile Red (NR) have a similar phenomenon (Figure S15, Supporting Information). Therefore, an orthogonal fluorescent “T” was observed at the angle of 0° (Figure 5b). The

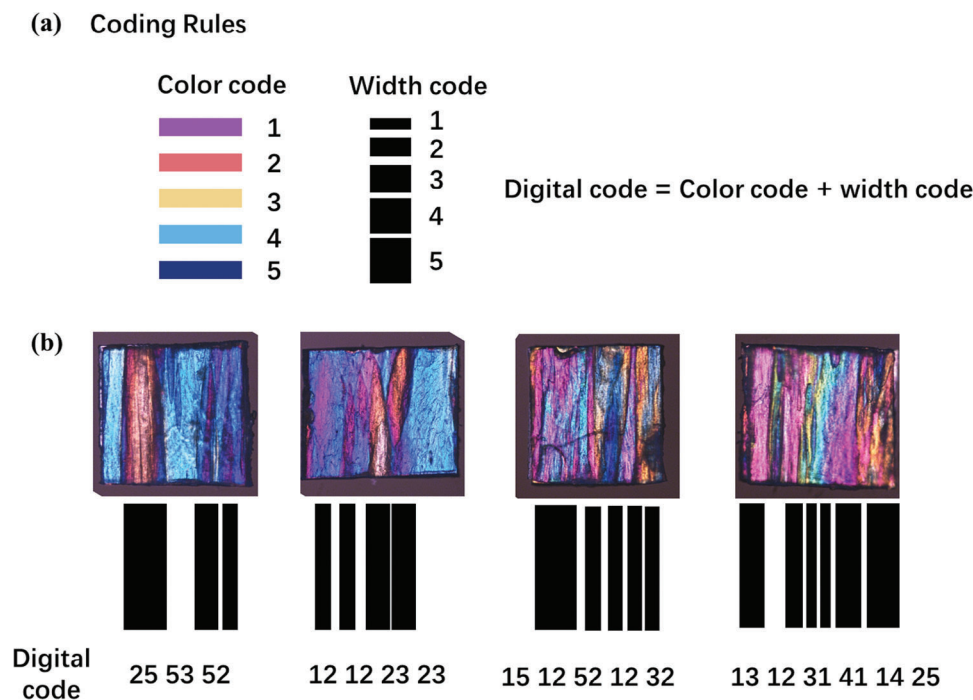


Figure 4. a) The mode and method for digital compilation of birefringence patterns. b) Digital compilation examples of birefringent patterns with gradually increasing complexity.

orthogonal birefringence and polarized fluorescence properties can be integrated for multi-logic information storage (Figure 5e), and any other forged similar patterns would be easily found to be fake by inputting the number code of each birefringence into the official website demonstrated in Figure 4. We expect the current strategy would offer an advanced anticounterfeiting technology for encryption and protection of valuable authentic information.

3. Conclusion

In summary, we have successfully constructed the Jun-porcelain like unduplicable birefringent anticounterfeiting film using the solid phase molecular self-assembly of anionic polyacrylamide and cationic surfactant cetyltrimethylammonium bromide (CTAB). The oppositely charged polyelectrolyte and surfactant would form precipitates upon mixing in water, and under mechanical pressure the molecules in the precipitates would rearrange to form a supramolecular film, where CTAB molecules predominantly pack into hexagonal crystal phases. Upon stretching, the CTAB crystal phases orient and merge into larger domains, which generate birefringence. Because of the inhomogeneous mass and molecular transportation in the solid phase, the large CTAB crystal domains are not uniform both in size and thickness and this occurs by chance, thus leading to unduplicable birefringence that is site and batch dependent. Overlaying the film or heating triggered CTAB crystal phase transition would further complicate the pattern. The polarization angle dependent birefringence also allows the generation of polarized fluorescence when fluorescent dyes are doped into the film, which gives the strongest fluorescence signal when the birefringence

is the weakest. The unduplicable orthogonal anticounterfeiting modes render the current Jun Porcelain like anticounterfeiting technique very appealing for encryption and protection of valuable authentic information.

4. Experimental Section

The Preparation of APAM-CTAB Film: To an aqueous solution of APAM, an aqueous solution of CTAB was added, reaching final concentrations of 50 mM for the negative charges of APAM and positive charges of CTAB. The white precipitates formed immediately after stirring and then centrifuged at 8000 rpm for 10 min in order to further remove the water in the precipitates. The collected precipitates were pressed by fingers to form transparent films.

Orientation of APAM-CTAB Films: The newly obtained APAM-CTAB film was first dried under ambient environment and then placed under 100% relative humidity environment for 1 day. Then a film with a certain orientation can be obtained by stretching with bare hands.

Analyzing Methods: X-ray diffraction (XRD) measurements were conducted using a Rigaku D/max-2400 diffractometer (Tokyo, Japan) with Cu K α radiation. 2D medium-angle X-ray scattering and wide-angle X-ray scattering (2D-MAXS, 2D-WAXS; Qingdao Jiuyi Graphite Co., Ltd., Shandong, China) patterns of the films, and the powders were recorded by a Ganesha SAXS system with a 2D detector. 2D-X-ray scattering at variable temperatures (25–80 °C) was controlled by a temperature control program. The temperature rising rate was 10 °C min⁻¹. Tests were conducted after 10 min of balancing. Polarized microscopy was obtained with an LV100N polarizing microscope (Nikon Co., Irving, CA) in ambient environmental conditions and elevated temperatures. The temperature rising and cooling rate was 10 °C min⁻¹. Samples were photographed with θ ranging from 0° to 359°, where θ was the angle between the analyzer and the alignment direction of the sample. Polarized ultraviolet-visible (UV-vis) spectroscopy measurements were conducted with a Shimadzu UV-3600 spectrometer by adding two polarizers with vertical polarization direction before and

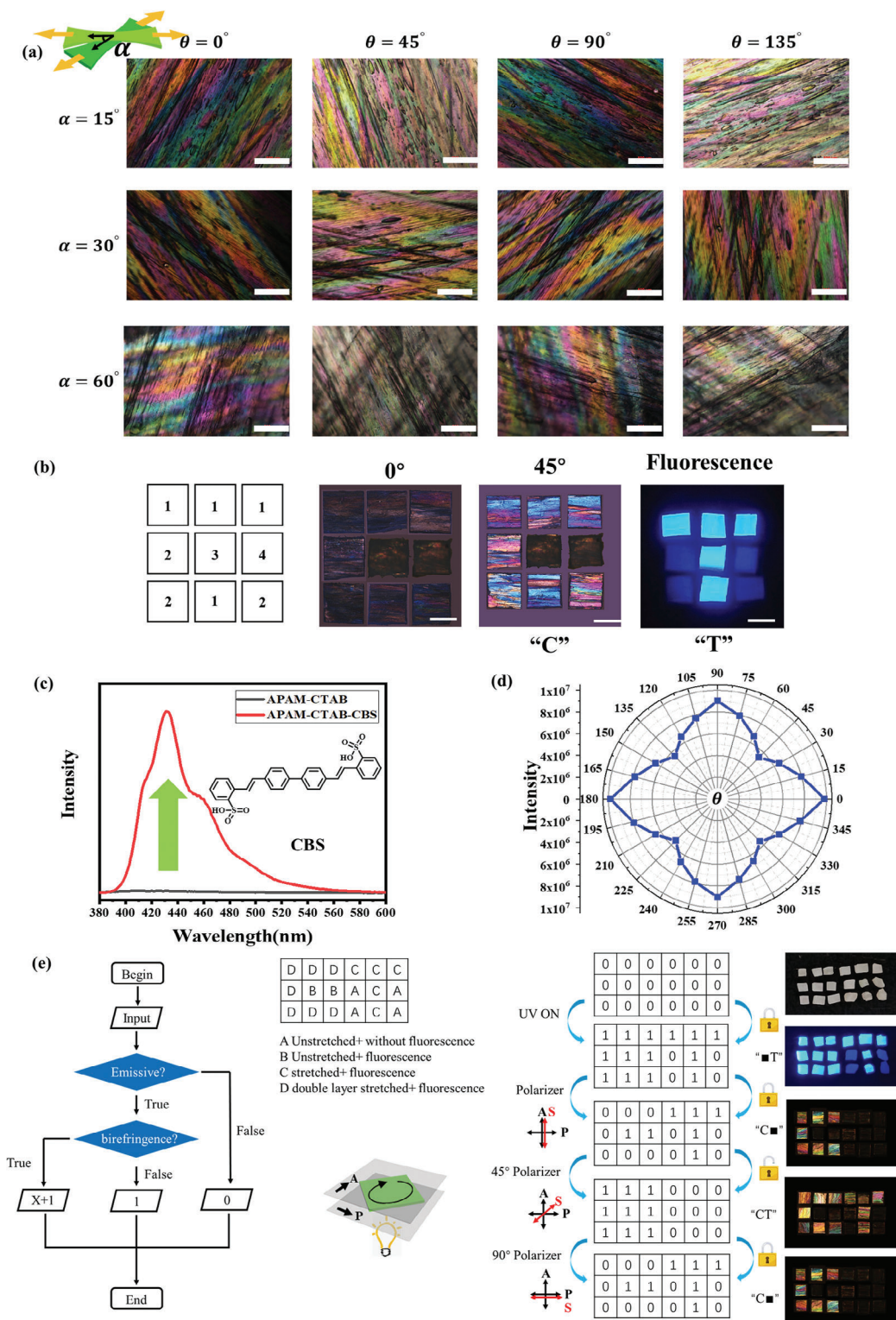


Figure 5. Application of birefringent film. Birefringence characteristics of two films stacked at different angles, a) variation of the birefringence pattern upon overlaying two stretched films at different angles. (Scale bar: 500 μm). b) Anticounterfeiting patens made with arrays composed of stretched and upstretched films. (1,2 are the stretched films; 3,4 are the unstretched ones; 1,3 are films doped with CBS). c) Fluorescence spectrum of APAM-CTAB-CBS ($E_x = 365 \text{ nm}$). d) Fluorescence intensity of APAM-CTAB-CBS film under different polarization angles. ($E_x = 365 \text{ nm}$, $E_m = 430 \text{ nm}$) (Due to the placement of the polarizer, when the polarization direction of the two polarizers is vertical, the luminous flux is reduced, causing the lower intensity at 90/270 degrees than that at 0/180 degrees.) e) Four-level logic anticounterfeiting enabled by integrating the polarized fluorescence and birefringence of the APAM-CTAB-CBS films. (In the experiment, the angle between the sample (S) and the polarizing plate (A, P) was rotated).

after the sample. The measurement mode was selected as the transmission mode. A series of transmission spectra can be obtained by changing the stretching direction of the film direction relative to the polarizer. The tensile measurement was performed using a WDW3020 electronic universal testing machine at a strain rate of 10 mm min⁻¹ with standard dumbbell shaped specimen of APAM-CTAB film. The CLSM experiments were conducted under fluorescence modes on A1R-si CLSM (Nikon, Japan) with 488 nm laser excitation. DSC measurement was conducted by Q2000 differential scanning calorimeter with a heating rate of 10 °C min⁻¹.

Supporting Information

Supporting Information is available from the Wiley Online Library or from the author.

Acknowledgements

The authors are grateful to National Natural Science Foundation of China (Grant No. 22332001, 22172004, 22202006), National Postdoctoral Researcher Program (GZC20230052), and the Beijing National Laboratory for Molecular Sciences (BNLMS) for financial support.

Conflict of Interest

The authors declare no conflict of interest.

Data Availability Statement

The data that support the findings of this study are available in the supplementary material of this article.

Keywords

anti-counterfeiting, birefringence, polyelectrolyte, self-assembly, surfactant

Received: December 10, 2024

Revised: January 19, 2025

Published online:

- [1] E. L. Prime, D. H. Solomon, *Angew. Chem.* **2010**, *49*, 3726.
- [2] J. Li, S. Xie, J. Meng, Y. Liu, Q. Zhan, Y. Zhang, L. Shui, G. Zhou, B. L. Feringa, J. Chen, *CCS Chem* **2024**, *6*, 427.
- [3] S. Huang, J. K. Wu, *IEEE Transactions on Information Forensics and Security* **2007**, *2*, 164.
- [4] M. Li, X. Yuan, H. Chen, J. Li, *IEEE Access* **2020**, *8*, 72308.
- [5] C. F. Wang, R. Cheng, W. Q. Ji, K. Ma, L. Ling, S. Chen, *ACS Appl. Mater. Interfaces* **2018**, *10*, 39205.
- [6] Z. Gao, Y. Han, F. Wang, *Nat. Commun.* **2018**, *9*, 3977.
- [7] H. Kang, J. W. Lee, Y. Nam, *ACS Appl. Mater. Interfaces* **2018**, *10*, 6764.
- [8] X. Wang, X. Chen, G. Xu, J. Li, J. Guo, Q. Wang, *Appl. Opt.* **2021**, *60*, 2304.
- [9] C. Li, X. Liu, Y. Han, Q. Guo, W. Yang, Q. Liu, B. Song, X. Zheng, S. Tao, *Cell Reports Physical Science* **2021**, *2*, 100571.
- [10] F. Zhang, W. Liang, L. Wang, Z. Ma, X. Ji, M. Wang, Y. Wang, X. Chen, D. Wu, X. Li, Y. Zhang, C. Shan, Z. Shi, *Adv. Funct. Mater.* **2021**, *31*, 2105771.
- [11] M. Zhang, M. Jia, T. Liang, Z. Wang, H. Xu, D. Duan, Y. Wei, Z. Fu, *J. Colloid Interface Sci.* **2022**, *608*, 758.
- [12] B. M. Oosterlaken, Y. Xu, M. M. J. Rijt, M. Pilz da Cunha, G. H. Timmermans, M. G. Debije, H. Friedrich, A. P. H. J. Schenning, N. A. J. M. Sommerdijk, *Adv. Funct. Mater.* **2019**, *30*, 1907456.
- [13] J. Guo, A. Tudi, S. Han, Z. Yang, S. Pan, *Angew. Chem.* **2019**, *58*, 17675.
- [14] H. Tian, C. Lin, X. Zhao, F. Xu, C. Wang, N. Ye, M. Luo, *CCS Chemistry* **2023**, *5*, 2497.
- [15] J. Zheng, X. Song, Y. Wu, Y. Lian, Y. Li, Q. Xu, Y. Zhou, Z. Wang, L. Wang, J. Luo, S. Zhao, *Adv. Funct. Mater.* **2024**, *34*, 2403843.
- [16] Y. Geng, R. Kizhakidathazhath, J. P. F. Lagerwall, *Nat. Mater.* **2022**, *21*, 1441.
- [17] H. Huang, X. Wang, J. Yu, Y. Chen, H. Ji, Y. Zhang, F. Rehfeldt, Y. Wang, K. Zhang, *ACS Nano* **2019**, *13*, 3867.
- [18] Y. Xiao, X. Lu, Y. Ma, Z. Chen, X. Shang, R. Hu, J. Ni, J. Dai, L. Liu, J. Mao, S. Yang, Y. Luo, *Chem. Eng. J.* **2024**, *493*, 152466.
- [19] X. Zhao, H. Feng, B. Yang, Y. Ma, X. Li, H. Chang, S. Tong, C. Xiong, Y. Luo, Z. Zhang, *J. Lumin.* **2023**, *264*, 120191.
- [20] X. Tang, L.-S. Cui, H.-C. Li, A. J. Gillett, F. Auras, Y.-K. Qu, C. Zhong, S. T. E. Jones, Z.-Q. Jiang, R. H. Friend, L.-S. Liao, *Nat. Mater.* **2020**, *19*, 1332.
- [21] S. Yook, S. Shams Es-Haghi, A. Yildirim, Z. Mutlu, M. Cakmak, *Soft Matter* **2019**, *15*, 9733.
- [22] K. Guo, W. Zhu, J. Wang, W. Sun, S. Zhou, M. He, *Carbohydr. Polym.* **2021**, *258*, 117694.
- [23] X. Li, X. Qiu, X. Yang, P. Zhou, Q. Guo, X. Zhang, *Adv. Mater.* **2024**, *2407170*.
- [24] W. Sun, Z. Song, J. Wang, Z. Yi, M. He, *Carbohydr. Polym.* **2024**, *332*, 121946.
- [25] X. Li, J. Liu, X. Zhang, *Adv. Funct. Mater.* **2023**, *33*, 2306208.
- [26] H. Liang, Y. Wu, Y. Zhang, E. Chen, Y. Wei, Y. Ji, *Adv. Mater.* **2023**, *35*, 2209853.
- [27] S. Wang, L. Lei, Y. Tian, H. Ning, N. Hu, P. Wu, H. Jiang, L. Zhang, X. Luo, F. Liu, R. Zou, J. Wen, X. Wu, C. Xiang, J. Liu, *Mater. Horiz.* **2024**, *11*, 2131.
- [28] W. Zhao, B. Wu, Z. Lei, P. Wu, *Angew. Chem., Int. Ed.* **2024**, *63*, 202400531.
- [29] H. Jin, C. Ma, W. Wang, Y. Cai, J. Qi, T. Wu, P. Liao, H. Li, Q. Zeng, M. Xie, J. Huang, Y. Yan, *ACS Mater. Lett.* **2022**, *4*, 145.
- [30] J. Qi, T. Wu, W. Wang, H. Jin, S. Gao, S. Jiang, J. Huang, Y. Yan, *Aggregate* **2022**, *3*, e173.
- [31] T. Wu, S. Gao, W. Wang, J. Huang, Y. Yan, *ACS Appl. Mater. Interfaces* **2021**, *13*, 41997.
- [32] P. Liao, S. Zang, T. Wu, H. Jin, W. Wang, J. Huang, B. Z. Tang, Y. Yan, *Nat. Commun.* **2021**, *12*, 5496.
- [33] W. Wang, M. Xie, H. Jin, W. Zhi, K. Liu, C. Ma, P. Liao, J. Huang, Y. Yan, *Mater. Chem. Front.* **2020**, *4*, 1530.
- [34] H. Jin, M. Xie, W. Wang, L. Jiang, W. Chang, Y. Sun, L. Xu, S. Zang, J. Huang, Y. Yan, L. Jiang, *CCS Chemistry* **2020**, *2*, 98.
- [35] C. K. Ober, G. Wegner, *Adv. Mater.* **1997**, *9*, 17.
- [36] S. Guillot, A. Chemelli, S. Bhattacharyya, F. Warmont, O. Glatter, *The Journal of Physical Chemistry B* **2009**, *113*, 15.
- [37] N. Martin, K. P. Sharma, R. L. Harniman, R. M. Richardson, R. J. Hutchings, D. Alibhai, M. Li, S. Mann, *Sci. Rep.* **2017**, *7*, 41327.
- [38] Z.-J. Sui, L. Vradman, I. Reizner, M. V. Landau, M. Herskowitz, *Catal. Commun.* **2011**, *12*, 1437.
- [39] C. Zhao, P. Zhang, J. Zhou, S. Qi, Y. Yamauchi, R. Shi, R. Fang, Y. Ishida, S. Wang, A. P. Tomsia, M. Liu, L. Jiang, *Nature* **2020**, *580*, 210.
- [40] M. M. Harding, *J. Synchrotron Radiat.* **1996**, *3*, 250.
- [41] W. J. Stroud, R. P. Millane, *Acta Crystallographica Section A Foundations of Crystallography* **1995**, *51*, 771.
- [42] O. Kose, A. Tran, L. Lewis, W. Y. Hamad, M. J. MacLachlan, *Nat. Commun.* **2019**, *10*, 510.